Optimisation of pulse shape discrimination using EJ299-33 for high energy neutron detection in proton beam therapy

S. Chung,[a] A. Kacperek,[b] R. Speller,[a] and A. Gutierrez [a]*

[a] *Department of Medical Physics and Biomedical Engineering, University College London University College London, Gower Street, London, WC1E 6BT*

[b] *The National Eye Proton Therapy Centre, Clatterbridge Cancer Centre NHS Foundation Trust Wirral, CH63 4JY, United Kingdom*

E-mail: a.gutierrez@ucl.ac.uk

ABSTRACT: It is widely understood that proton beam therapy has considerable clinical benefits over photon therapy for treating certain types of tumours. Protons deposit most of their energy in a very localised area, the so-called Bragg peak, sparing surrounding healthy tissue and critical organs from radiation. However, secondary neutrons and gamma rays are generated in the beam nozzle and inside the patient. Clinically, it is highly desirable to monitor the neutron dose the patient is exposed to, and this requires a neutron detector sensitive to high energies. EJ299-33 is a solid plastic scintillator capable of discriminating neutrons from gamma rays using pulse shape analysis of scintillation light. EJ299-33 has the potential to detect neutrons with energies up to 100 MeV and does not present leakage and flammability hazards generally associated with liquid scintillators. Experimental measurements with ^{60}Co, ^{137}Cs and ^{241}AmBe sources were performed to calibrate and optimise pulse shape discrimination parameters. We also performed experimental measurements at the Clatterbridge Cancer Centre in a 60 MeV passive scattered beam to detect high energy neutrons.

KEYWORDS: Neutrons, Organic plastic scintillator, EJ299-33, Proton beam therapy

* Corresponding author.

Contents

1. Introduction

Proton therapy draws growing attention worldwide because of its significant integral dose reduction. However, secondary particles such as neutrons and gamma rays are generated due to proton inelastic nuclear interactions with the beam nozzle and patients. Neutron energy ranges from thermal up to the proton beam energy [1]. They are hazardous as the biological effect of 1 MeV neutrons is roughly 20 times higher than 1 MeV photons [2]. This raises radiation safety concerns associated with the induction of secondary cancers, especially for paediatric patients, since secondary cancers tend to appear after a few decades after irradiation [3].

A variety of neutron studies during proton beam therapy have been carried out using detectors such as Bonner sphere spectrometers (BSS) [4, 5], ^{3}He proportional counters [6] and WENDI-2 dosimeters [5]. A detector, which can detect high energy neutrons and measure the neutron energy spectrum, is highly desirable as the neutron energy distribution changes with the direction from the beam axis.

In 2012, the use of a solid organic plastic scintillator (Eljen EJ299-33) for the detection of neutron and gamma fields with pulse shape discrimination (PSD) technique was first reported [7]. This scintillator has the potential of measuring neutron energies up to 100 MeV [8]. Moreover, it has the additional merit of being free of safety hazards associated with liquid scintillators (e.g. leakage, flammability and toxicity).

In this work, we investigate optimising the PSD parameters of EJ299-33 organic plastic scintillator for the detection of secondary neutrons in proton beam therapy using the RadICAL technique [9].

2. Methodology

This part includes the description of the detector assembly, PSD technique and the Figure of Merit (FoM) to quantify its performance.

2.1 Detector assembly and readout

The scintillator is 11 cm×2.5 cm×1.5 cm and one end of the scintillator is coupled to an ET Enterprise 9102B photomultiplier tube (PMT). The system is assembled inside a plastic enclosure, as shown in Figure 1a. The dimensions of the scintillator were optimized as for the RadICAL (Radiation Imaging Cylinder Activity Locator) system, where a long, thin rotating scintillator provides information to locate a radiation source [9, 10]. The PMT high voltage is supplied by a CAEN V6533N module and the signal output is analysed by a CAEN V1751 digitiser, with online digital pulse processing performed by a field-programmable gate array (FPGA). A CAEN V1718 module is used to communicate with a PC and the modules are powered by a CAEN VME8004B crate, as illustrated in Figure 1b.

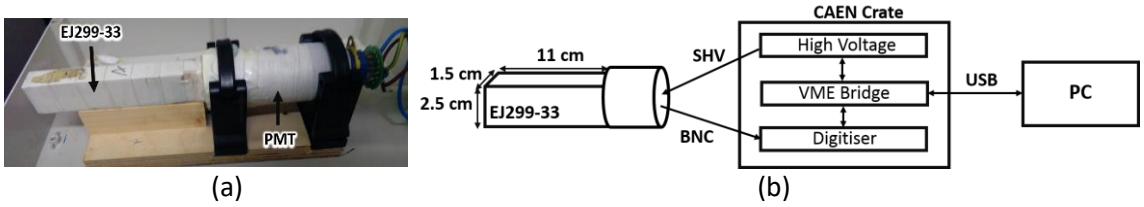

Figure 1. a) The scintillator and PMT assembly. b) Illustration of the detection system (not to scale).

2.2 Pulse shape discrimination (PSD) technique

The PSD technique relies on the different shapes as a function of time of the pulses of scintillation light produced by different particles. Gamma rays and fast neutrons interact differently in the scintillator: gamma rays produce secondary electrons mainly via Compton scattering, while fast neutrons undergo elastic interactions with hydrogen nuclei, producing recoil protons. Secondary electrons and recoil protons both produce a prompt fluorencense (tens of nanonseconds) in the scintillator, but due to the higher LET of protons, there is an important delayed fluorescence (hundereds of nanonseconds) that can be used in the pulse analysis to differentiate neutrons from gamma rays [11].

An example of the different pulse shapes of gamma rays and neutrons is illustrated in Figure 2. Two simultaneous but varying time gates, T_{short} and T_{long}, are used to collect the integrated signal from the PMT, Q_{short} and Q_{long}, respectively. Q_{short} is mainly the fast component of the signal, whereas Q_{long} is the total charge of the pulse. The PSD is the ratio of the slow component, Q_{tail}, (i.e. $Q_{long} - Q_{short}$), to the total charge, as shown in equation 1. Thus if a mixed neutron-gamma field is studied, a histogram of PSD values will have two peaks.

$$PSD = \frac{Q_{long} - Q_{short}}{Q_{long}} \quad \text{Equation 1}$$

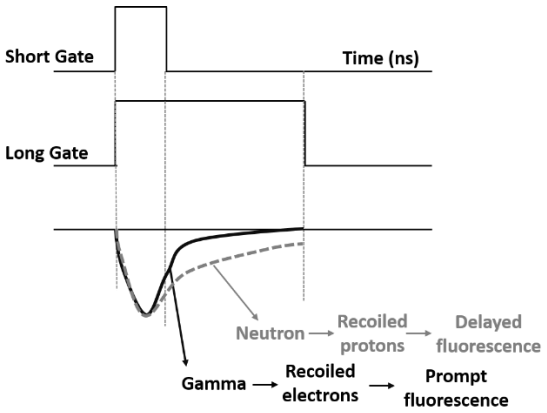

Figure 2. Illustration of PSD principle for a neutron and a gamma ray.

2.3 A Figure of Merit (FoM) for quantifying PSD performance

A FoM can be used to quantify the PSD peformance of the detector. The FoM is defined as the ratio of the separation between the neutron and gamma peaks to the sum of their Full Width Half Maxima (FWHM), as shown in equation 2 and illustrated in Figure 3. Two Gaussian fits are performed, where the difference between the mean of the two distributions is the separation and the FWHM is calculated as $2\sqrt{2\ln 2}\,\sigma$, where σ is the Gausssian standard deviation. The higher the FoM, the better the discrimination between neutron and gamma signals. Also, an energy threshold can be applied to improve the PSD performance.

$$FoM = \frac{Separation}{FWHM_{gamma}+FWHM_{neutron}} \qquad \text{Equation 2}$$

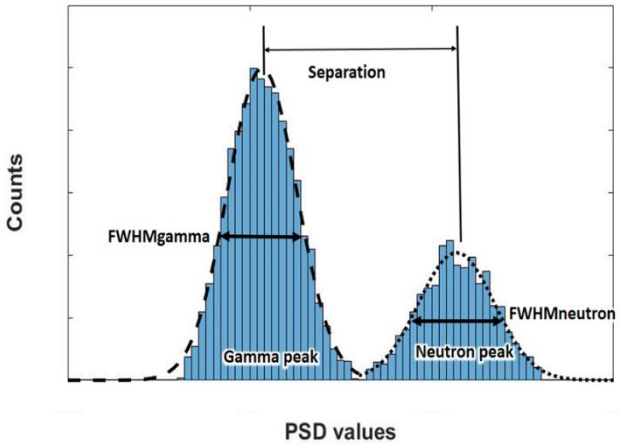

Figure 3. Illustration of the FoM parameters for the assessment of the goodness of the discrimination between gamma rays and neutrons.

We performed experimental measurements using gamma sources for energy calibration, mixed neutron-gamma fields from ^{241}AmBe source to optimize the PSD parameters and performed measurements of neutron-gamma fields generated during proton beam therapy. In all cases, the long axis of the scintillator was perpendicular to the beam or sources.

3. Results and discussion

3.1 Energy calibration with gamma sources

To calibrate the detector, ^{60}Co and ^{137}Cs gamma sources were used. Due to the dimensions of the scintillator, it can be assumed that gamma rays lose their energy mainly by Compton scattering, and thus the Compton edge has been used for calibration purposes. The sources were placed on the top of the scintillator and two different PMT voltages, 800 V and 900 V, were applied. The theoretical Compton edge was calculated to be 447 keV and 1041 keV for ^{137}Cs and ^{60}Co, respectively. Since the detector has in general a poor energy resolution, for ^{60}Co, we use the average energy of the 1173 keV and 1333 keV peaks. The Compton edge was calculated by performing a linear fit at the right edge of the total charge (Q_{long}) histogram, which represents the Compton continuum. The Compton edge was defined when the 80% of the edge maximum is reached [12, 13], as shown in Figure 4a. Figure 4b shows the linear fits for energy calibration at 800 V and 900 V.

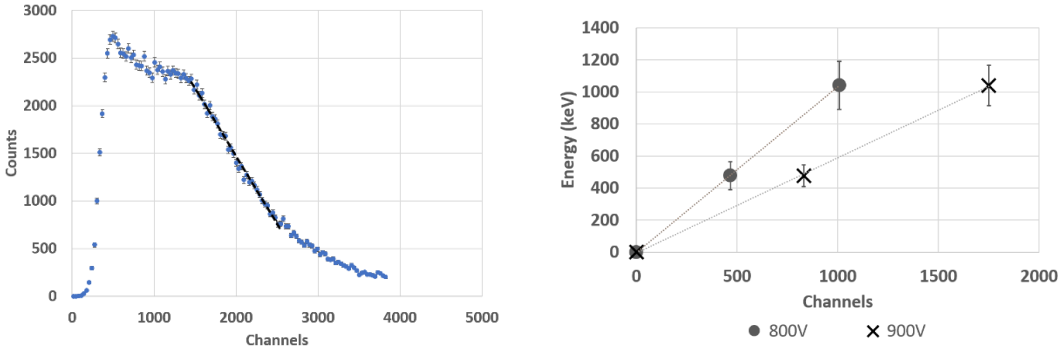

(a) (b)

Figure 4. a) Compton edge determination from a ^{60}Co energy histogram at 900V with Poisson error bars. b) Energy calibration using ^{60}Co and ^{137}Cs gamma sources. The errors are calculated from the linear fit performed in a).

We used the fits in Figure 4b to extrapolate the energy to the last channel. The limit, which is given in electron equivalent energy (amount of energy converted to light by recoil electrons), is ~20 MeVee at 900 V and ~34 MeVee at 800 V. Since the energy calibration was performed using gamma rays, the neutron energy might not follow the same gamma energy scale. In this paper we use both voltages to investigate the neutron response of the detector.

3.2 Neutron-gamma PSD with ^{241}AmBe source

Experimental measurements with a ^{241}AmBe source were performed at the Central Teaching Hub of the University of Liverpool. The source was placed at one side of the water tank and a 4 mm thick cadmium sheet was used to shield the detector from low energy neutrons (below 0.5 eV), as shown in Figure 5.

Figure 6a shows a PSD histogram with its Gaussian fit when the detector was exposed to the source. The FoM was found to be 0.85 ± 0.01 when using a threshold of 3 MeVee. Figure 6b shows a scatter plot of the PSD as function of Q_{long}. We can see a high concentration of events at low energy and events are better discriminated at high energy. This will be to our advantage since we are interested in fast neutron detection and we can discard low energy particles.

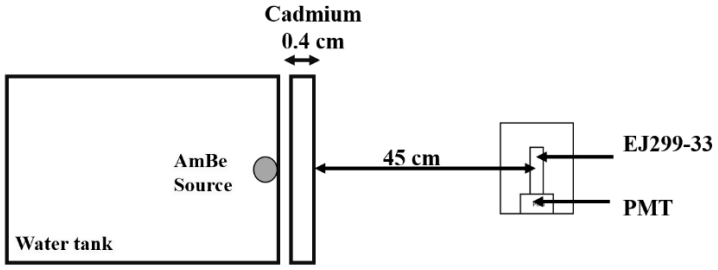

Figure 5. Illustration of the neutron-gamma measurements with an ^{241}AmBe source (top view and not to scale).

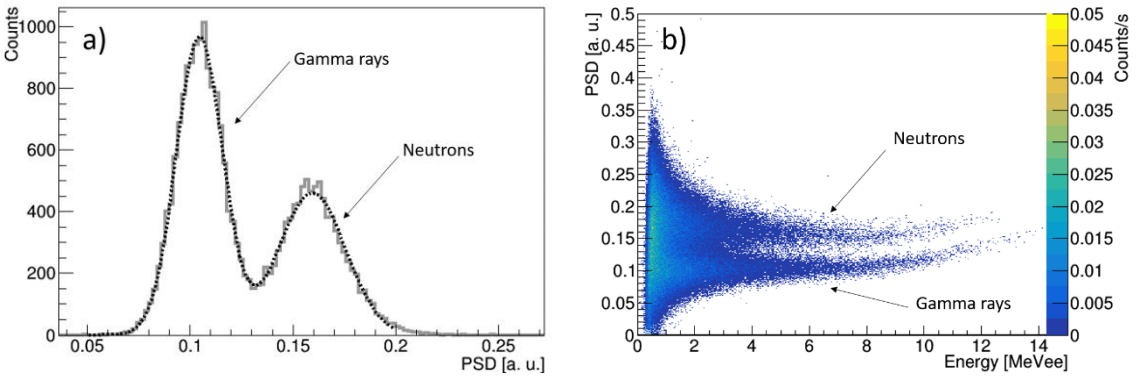

Figure 6. a) Histogram of PSD values (solid line) with two Gaussian fits (dotted line) to calculate the FoM using a 3 MeV threshold. b) 2D scatter of PSD values as a function of energy. The voltage was fixed at 800 V, T_{short} at 52 ns and T_{Long} at 320 ns. For these measurements, 10 cm of lead was used to shield the detector from low energy gamma rays.

We studied the effects of changing the timing gate durations, T_{short} and T_{long}, independently. In Figure 7a, we used T_{short} = 28 ns and we observe poor discrimination between neutrons and gamma rays. Furthermore, there is an obvious bend for gamma rays above ~5 MeVee. This could be caused by three possible reasons. Firstly, the distortion can be attributed to a saturation in the photomultiplier system [14]. Secondly, the relation between light output and energy deposited in EJ299-33 is not linear. In fact, it increases exponentially when more energy is deposited in the scintillator [15]. Thirdly, it could be possible that high energy neutrons might have a different pulse shape than low energy neutrons (e.g. other fluorescence components become more prominent) such that the short gate is optimised for lower energy neutrons rather than higher energy neutrons. This could be supported by the fact that a deep bend is observed in 28 ns T_{short} and a shallow bend is found in 102 ns $T_{short.}$ On the other hand, if T_{short} is above ~100 ns, Q_{tail} considerably decreases and the overall PSD values are too low, resulting in missed information from low energy particles, as shown in Figure 7b.

When using a Q_{long} of about 320 ns (see Figure 8a), the PSD range becomes narrower, while a longer Q_{long} creates a broader PSD range as shown in Figure 8b. However, the Q_{long} duration does not make a significant difference since the slow component of the pulse is already included in Q_{tail} at these energies.

A T_{short} of around 50 ns seems to be reasonable for the discrimination of neutron-gamma and a T_{long} of 500 ns seems to be conservative to collect the slow fluorescence components. In the

following section we will discuss the measurements made with a neutron-gamma mixed field during proton beam therapy.

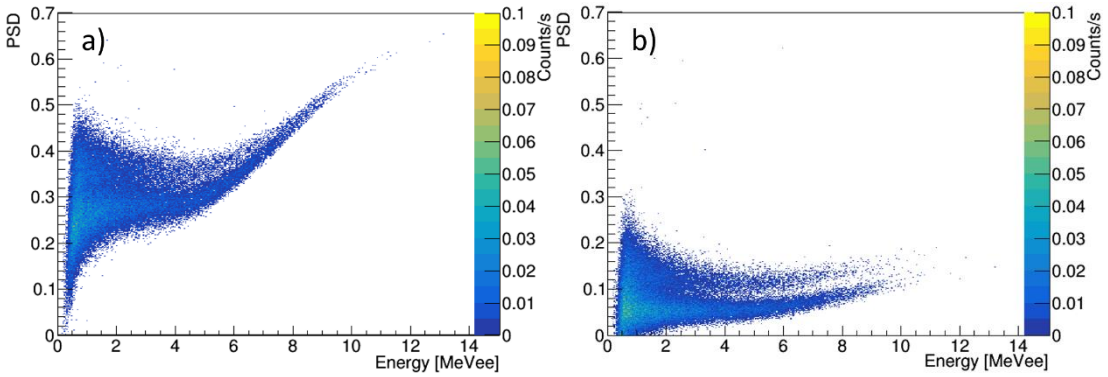

Figure 7. 2D scatter plots of PSD as a function of energy when a) T_{short} = 28 ns and b) T_{short} = 102 ns. The voltage was fixed at 900 V and T_{long} at 500 ns.

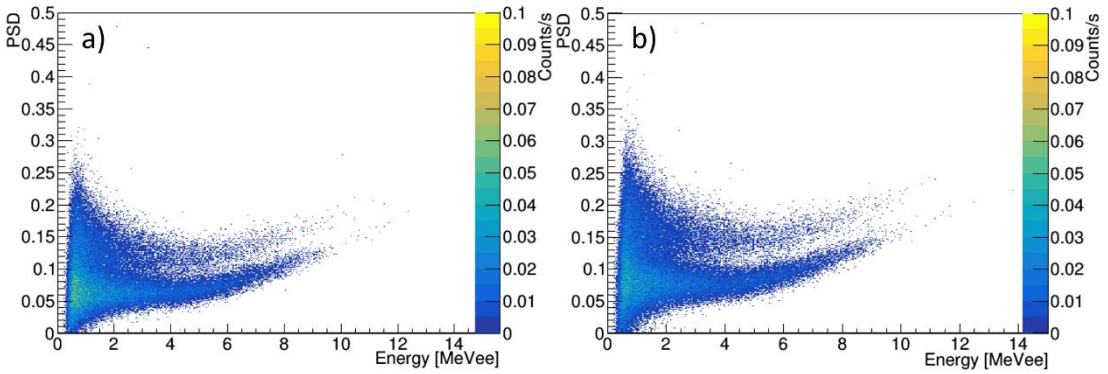

Figure 8. 2D scatter plots of PSD as a function of energy when a) T_{long} = 320 ns and b) T_{long} = 520 ns. The voltage was fixed at 900 V and T_{short} at 74 ns.

3.3 Secondary neutron measurements with a 60 MeV proton beam

Secondary neutrons generated by a 60 MeV passive scattered proton beam were measured at the National Eye Proton Therapy Centre at the Clatterbridge Cancer Centre [16]. Firstly, we performed measurements of secondary neutrons with a completely blocked nozzle, to simulate the maximum neutron flux and secondly, we irradiated a paraffin target with protons and placed the detector at different angles around the phantom.

3.3.1 Secondary neutrons from protons stopped at the beam nozzle

To maximize the generation of secondary neutrons in the nozzle, we used a 3 mm diameter brass collimator blocked with a brass stopper, as shown in Figure 9. The scintillator was positioned perpendicular to the beam line 100 cm from the nozzle. The neutron energy should range up to 60 MeV, but due to our PMT limitations, we are only able to detect neutrons up to ~35 MeVee.

We observed mainly neutrons in this measurement. We believe that gamma rays produced in the nozzle are present, but in the background. There is a drastic change above ~12 MeVee on the PSD values where they become linear as a function of energy. This could indicate that as the energy of the particle increases, Q_{tail} becomes more important. Besides the possible reasons discussed in

section 3.2, we also need to take into account that the interaction of neutrons in the scintillator is complex. Recoil protons are produced after elastic collisions with ^{1}H and the energy transferred to the protons by the neutrons depends on the scattering angle, which results in a wide energy distribution of recoil protons. Furthermore, some recoil protons are likely to escape the scintillator, depending on the locations of the elastic collisions and their energy. A characterization of these interactions is still needed. Further improvements can be made by using a photomultiplier with a lower gain.

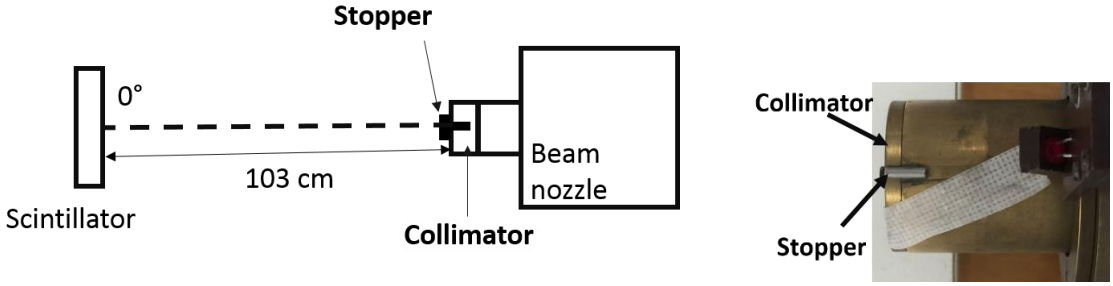

Figure 9: a) Experimental setup of a 60 MeV proton beam line with a blocked collimator (not to scale). b) A top view of 3 mm collimator and its stopper.

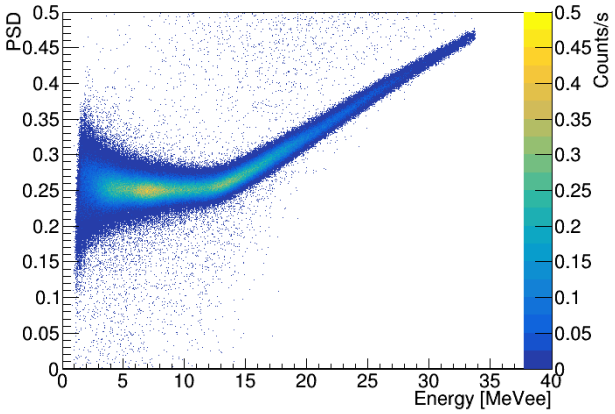

Figure 10. 2D scatter plots of PSD as a function of energy at 800 V. T_{short} was fixed at 52 ns and T_{long} at 500 ns.

3.3.2 Secondary neutrons from proton irradiation of a paraffin phantom

A cylindrical paraffin phantom (10 cm diameter and 19 cm height) was placed 20 cm from the nozzle. We used a 1.5 cm diameter brass collimator for the proton beam and the scintillator was placed ~135 cm from the phantom at 15° and 50° from the beam axis as shown in Figure 11. The phantom was irradiated with ~1.5×10^{9} protons.

Figure 12 shows the 2D scatter plots for the PSD when the detector was placed a different angle. For both plots, we can see two distributions, where the gamma ray energy goes up to around 12 MeVee and the neutron distribution up to the energy limit of the detector. As the previous measurement, we observe a bend of the PSD distribution above 12 MeVee. A larger number of high energy neutrons is detected when the detector is placed at 15° to the beam line. This is because neutrons are mostly produced in the forward direction [17]. During these measurements,

neutrons are produced in the beam nozzle and the phantom. Further measurements and simulations are needed to analyse the effect and the location of neutron generation.

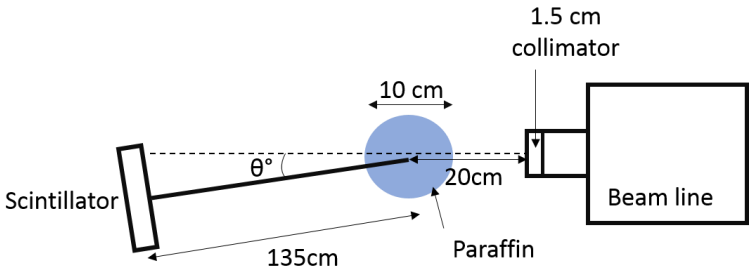

Figure 11: Experimental setup of a 60 MeV proton beam line with a 1.5 cm collimator and a paraffin phantom (not to scale).

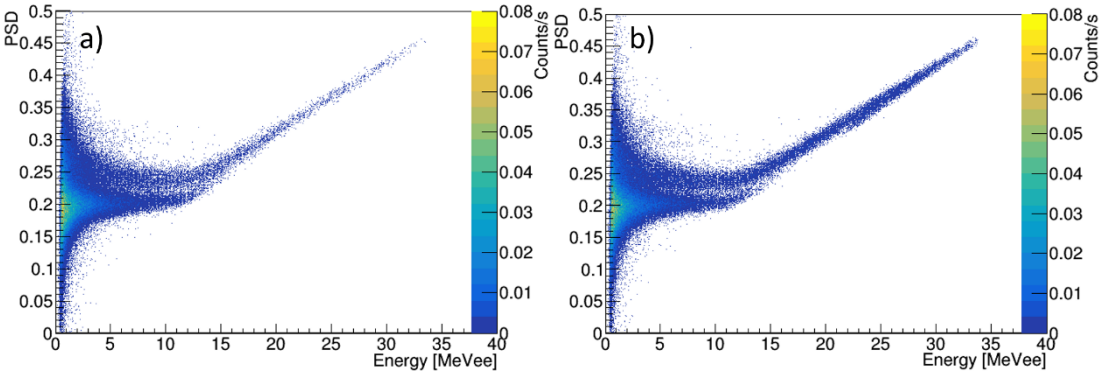

Figure 12. 2D scatter plots of PSD as a function of energy when the detector is placed at a) 50° and b) 15° from the beam line. The voltage was fixed at 800 V, T_{short} at 52 ns, and T_{long} at 320 ns.

4. Conclusion

We characterised and optimised EJ299-33 detector for the discrimination of neutron-gamma radiation during proton beam therapy. We detected neutron energies up to ~35 MeVee and gamma rays up to ~12 MeVee. However, simulations are needed to further study the neutron energy calibration. Further measurements are needed to investigate the capability of the detector to locate the neutron source (e.g. beam nozzle, phantom) similarly to the RadICAL system.

5. Acknowledgments

The authors acknowledge the staff at the Clatterbridge Cancer Centre and the Central Teaching Hub of the University of Liverpool for their help during data collection.

6. References

[1] R.M. Howell and E.A. Burgett, *Secondary neutron spectrum from 250-MeV passively scattered proton therapy: measurement with an extended-range Bonner sphere system, Med. Phys.* **41** (2014) 092104.

[2] N. Petoussi-Henss, et al., *Conversion coefficients for radiological protection quantities for external radiation exposures.* ICRP Publication 116 (2010).

[3] X.G. Xu, B. Bednarz and H. Paganetti, *A review of dosimetry studies on external-beam radiation treatment with respect to second cancer induction, Phys. Med. Biol.* **53** (2008) R193.

[4] R.M. Howell, et al., *Measured neutron spectra and dose equivalents from a Mevion single-room, passively scattered proton system used for craniospinal irradiation, Int. J. Radiat. Oncol. Biol. Phys.* ***95(1)*** *(2016) 249-57.*
[5] M. De Saint-Hubert, et al., *Secondary Neutron Doses in a Proton Therapy Centre, Radiat. Prot. Dosimetry.* **170** (2016) 336-41.
[6] S.E. Han, G. Cho and S.B. Lee, *An Assessment of the Secondary Neutron Dose in the Passive Scattering Proton Beam Facility of the National Cancer Center, Nucl. Eng. Technol.* **46** (2016) 801-809.
[7] N. Zaitseva, et al., *Plastic scintillators with efficient neutron/gamma pulse shape discrimination, Nucl. Instrum. Meth. A.* **668** (2012) 88-93.
[8] A. Buffler, et al., *Neutron Spectrometry with EJ299-33 Plastic Scintillator for En = 10-100 MeV. IEEE Tran. Nucl. Sci.* **62** (2015) 1422.
[9] G.L. Randall, et al., *A method of providing directionality for ionising radiation detectors – RadICAL, J. Instrum*. (2014) 9.
[10] C. Payne, et al., *Neutron/gamma pulse shape discrimination in EJ-299-34 at high flux,* in *Proc. IEEE NSS/MIC,* San Diego CA U.S.A, 31 October - 7 November (2015).
[11] G.H.V. Bertrand, M. Hamel and S. Normand et al., *Pulse shape discrimination between (fast or thermal) neutrons and gamma rays with plastic scintillators: State of the art. Nucl. Instrum. Meth. A.* **766** (2015) 114.
[12] J. Iwanowska-Hanke, et al., *Comparative study of large samples (2" × 2") plastic scintillators and EJ309 liquid with pulse shape discrimination (PSD) capabilities, J. Instrum.* **9** (2014) P06014 .
[13] M. Monterial, et al., *Application of Bayes' theorem for pulse shape discrimination, Nucl. Instrum. Meth. A.* **795** (2015) 318.
[14] C. Liao and H. Yang, *Pulse shape discrimination using EJ-299-33 plastic scintillator coupled with a Silicon Photomultiplier array, Nucl Instrum Methods Phys Res A.* **789** (2015) 105.
[15] C.C. Lawrence, et al., *Neutron response characterization for an EJ299-33 plastic scintillation detector, Nucl Instrum Methods Phys Res A.* **759** (2014) 16.
[16] A. Kacperek, *Protontherapy of eye tumours in the UK: A review of treatment at Clatterbridge, Appl Radiat Isot.* **67** (2009) 378-386.
[17] D. Shin, et al., *Secondary neutron doses for several beam configurations for proton therapy. Int J Radiat Oncol Biol Phys.* **74** (2009) 260.